

Atomic and Electronic Structures of 6H-SiC(000 $\bar{1}$)-3 \times 3 Surfaces

F. Takeuchi¹, R. Fukuyama¹, Y. Hoshino², T. Nishimura¹ and Y. Kido¹

Abstract

The atomic and electronic structures of 6H-SiC(000 $\bar{1}$)-3 \times 3 reconstructions were analyzed by high-resolution medium energy ion scattering (MEIS) combined with photoelectron spectroscopy. We prepared three types of (3 \times 3) surfaces by (a) annealing the Si-rich (2 \times 2) surface at 1030°C, (b) annealing the $\sqrt{3} \times \sqrt{3}$ silicate surface at 1050°C, and (c) annealing the RCA-treated surface at 1050 °C in ultrahigh vacuum. The present MEIS analysis reveals the fact that the (3 \times 3) surfaces consist of a Si-adlayer(1.1 ML), C-adlayer(0.5 ML) and C-adatoms(1/3 ML)/C-adlayer(2/3 ML) on the 1st C-Si bilayer for samples (a), (b) and (c), respectively. Observation of the valence band spectra shows that all the surfaces are semiconducting and have dangling bond states in the band gap (1.4 eV below the Fermi level for sample (a)). The Si-rich surface (a) has one surface-related component in Si 2p and in contrast, the C-rich surfaces ((b) and (c)) have two surface-related components in C 1s spectra. It is shown that the (3 \times 3) reconstructions of the SiC(000 $\bar{1}$) are categorized into the above three types and take different atomic configurations. For the Si-rich (3 \times 3) surface, the present analysis supports the structure model proposed by Hoster et al.(Surf. Sci. **382** (1997) L658). The probable structures of the C-rich (3 \times 3) surfaces are also discussed in detail.

¹ Department of Physics, Ritsumeikan University, Kusatsu, Shiga-ken 525-8577, Japan

² Department of Electronic Science and Engineering, Kyoto University, Katsura, Kyoto 615-8510, Japan

I. INTRODUCTION

It is well known that silicon carbide crystals take a variety of surface reconstructions. For the $\text{SiC}(000\bar{1})$ surface terminated with C, Johansson et al.[1] reported that heating the as-introduced sample at 1050°C in ultra-high vacuum (UHV) led to formation of a (3×3) structure and further heating at a higher temperature of 1200°C resulted in surface graphitization. The (3×3) surface reconstruction was also observed by annealing the $(\sqrt{3}\times\sqrt{3})$ silicate surface at 1050°C for 15 min in UHV and annealing at a higher temperature of 1075°C led to a C-rich (2×2) reconstruction[2,3]. Forbeaux et al.[4] observed the (3×3) surface by annealing the as-introduced sample at 950°C with an Si flux. Further annealing the surface at 1050°C led to the (2×2) reconstruction. Recently, Sieber et al.[5] passivated the surface with hydrogen and heated the surface at 950°C in UHV to form the (3×3) reconstruction. Concerning the probable surface structure, Hoster et al.[6] proposed a model that the (3×3) surface takes a hexagonal unit cell consisting of a central trimer bonded to underlying six-atom dimmers rings based on the scanning tunneling microscope (STM) observation. However, it is still unknown whether all the above (3×3) surfaces take a same structure or not.

The aim of this work is to answer the above question and if not the same to categorize the $\text{SiC}(000\bar{1})$ - 3×3 surfaces reported so far. We prepared the $\text{SiC}(000\bar{1})$ - 3×3 surfaces by three different methods, (a) annealing the Si-rich (2×2) surface[7] at 1030°C , (b) annealing the $(\sqrt{3}\times\sqrt{3})$ silicate surface at 1050°C , and (c) annealing the RCA-treated[8] surface at 1050°C in UHV without Si pre-deposition. The reconstructed surfaces were analyzed by high-resolution medium energy ion scattering (MEIS) coupled with photoelectron spectroscopy (PES) using synchrotron-radiation (SR) light. The present MEIS analysis identifies the atomic species of the reconstructed surface and determines the absolute amounts of the adatoms/adlayer. We also observed the core level spectra of C 1s and Si 2p together with the valence band spectra. The PES analysis gives information about the bonding states and the electronic nature of the surfaces, which are intimately related to the surface structure. Finally, we discuss the probable surface structure considering the above

observations.

II. EXPERIMENT

In the present experiment, on-axis N-doped 6H-SiC(000 $\bar{1}$) substrates purchased from CREE corporation were used. The surfaces were treated by chemical and mechanical processing (CMP) and thus uniformly flat without any scratching. After RCA cleaning[8], we introduced the sample with a size of 10×10 mm² into an UHV chamber and performed degassing at 600 °C for 5 h with an infrared radiation heater. Then the (3×3) surfaces were prepared by the following three different methods. We first pre-deposited a small amount of Si (3 ML, 1 ML for SiC(0001): 1.21×10¹⁵ atoms/cm²) and then annealed at 950 °C for 5 min to form the Si-rich (2×2) reconstruction, whose structure was determined previously[7]. Further annealing at 1030 °C for 5 min changed the surface into a (3×3) structure (a). Reflection high energy electron diffraction (RHEED) showed a sharp (3×3) pattern with strong Kikuchi lines. The surface heated at a higher temperature of 1100 °C exhibited a (2×2) reconstruction, which corresponds to the C-rich surface, as reported by Bernhardt et al.[2,3] and Forbeaux et al.[4]. The second (3×3) sample (b) was obtained by annealing the ($\sqrt{3} \times \sqrt{3}$) silicate surface at 1050 °C which was grown by oxidizing the Si-rich (2×2) surface at 500 °C [9]. Further annealing at a higher temperature of 1100 °C led to coexistence of the (3×3) and (2×2) reconstructions. The (3×3) surface was also formed by annealing the de-gassed surface at 1050 °C for 15 min in UHV without Si-predeposition (c). This treatment resembles that reported by Johansson et al.[1].

All the analyses were carried out *in situ* at beam line 8 named SORIS at Ritsumeikan SR Center working under UHV conditions ($\leq 2 \times 10^{-10}$ Torr)[10]. Well collimated He⁺ ions with an energy of 120 keV were incident along the axis making an angle of 54.7° with respect to surface normal in the (11 $\bar{2}$ 0) plane to suppress background (channeling condition). Backscattered He⁺ ions were energy-analyzed by a toroidal electrostatic analyzer (ESA) combined with three-stage micro-channel plates (MCP) connected to a position sensitive detector (PSD), which gives an excellent energy resolution ($\Delta E / E$) of

9×10^{-4} . The observed MEIS spectrum was best-fitted by simulated one assuming an appropriate layered structure. The stopping powers of C and Si for medium energy He ions were determined in advance using a graphite film and a poly crystal Si layers stacked on SiO₂/Si(111) whose thickness was measured by Rutherford backscattering with 1.5 MeV He⁺ ions. As the energy straggling values, we employed the Lindhard-Scharff formula[11]. For reliable analysis, it is indispensable to have the knowledge of the He⁺ fractions dependent on the emerging velocity, surface materials, and emerging angle. In particular, for the scattering components from top layer atoms at a small emerging angle scaled from surface normal, the He⁺ fractions are not equilibrated and significantly larger than equilibrium fractions[12]. We determined experimentally the equilibrium and non-equilibrium He⁺ fractions for graphite and the poly crystal Si film stacked on SiO₂/Si. Here, it must be noted that only He⁺ ions were detected with the toroidal ESA. In the present MEIS experiment, integrated beam current was measured precisely by applying a voltage of + 90 V to the sample to suppress secondary electrons emission. Another crucial point is the asymmetric nature of the energy spectra in particular from a subsurface area originating from inner shell excitations[13]. This gives some uncertainty in determining the absolute amounts of C and Si adatoms. The cross sections of inner shell excitations depend on the incident ion velocity. For medium energy He⁺ ions, the asymmetric effect is expected to be not very pronounced. In the present MEIS analysis, we used asymmetric Gaussian shapes for each scattering component from subsurface layers[14]. The detection efficiency of the MCP/PSD system was estimated to be 0.52 ± 0.02 [12].

The storage ring named AURORA provided intense and polarized photons, which were monochromated with two kinds of gratings in the energy range from 10 to 500 eV. For the grating covering the energy range from 10 to 150 eV, the incident photon energy was calibrated exactly using the second harmonic wave. We observed the C 1s and Si 2p_{1/2,3/2} core levels together with valence band spectra by a hemispherical ESA with a mean curvature of 137.9 mm. The system energy resolution was estimated to be about ± 0.05 eV at a pass energy of 2.95 eV. Observed spectra were normalized from an integrated beam

current of an Au mesh placed in front of a sample.

III. RESULTS AND DISCUSSION

A. MEIS Analysis

Figure 1 shows the MEIS spectra observed for 120 keV He^+ ions incident at 54.7° and backscattered from the (3×3) surfaces (a)-(c). In order to get a good depth resolution, we set glancing emergence geometries. The vertical dash-dotted lines indicate the energy positions for the He^+ ions backscattered from C and Si atoms assumed on top of the surface (surface front edge). The solid and dashed curves are the simulated spectra best-fitted to the observed ones. Here, we used the ZBL potential[15] to calculate the scattering cross sections. For the sample (a), the top surface consists of a Si-adlayer of 1.1 ± 0.05 ML on the 1st C-Si bilayer. Here, an adatoms/adlayer structure was not resolved probably due to slight difference in their height. The 1st C-Si bilayer (thick dashed curves) is completely visible from the incident He^+ ions but the scattering components from the underlying C-Si bilayers (2nd, 3rd, ... C-Si bilayers: thin solid curves) are significantly shadowed along incoming and outgoing trajectories. The Si-adlayer seems to shadow the 2nd C-Si bilayer to some extent. For the samples (b) and (c), however, C-adlayers with a coverage of 0.5 ± 0.1 and 1.0 ± 0.1 ML, respectively are located on the 1st C-Si bilayer. It is quite interesting that for the sample (c) the surface component (1.0 ± 0.1 ML) is deconvoluted into two parts, (i) C-adatoms ($1/3$ ML) on top and (ii) underlying C-adlayer ($2/3$ ML). For both samples (b) and (c), no shadowing effect is seen for the 1st C-Si bilayer but the underlying C-Si bilayers (thin solid curves) are shadowed slightly. The diminished shadowing effect is due to smaller Z number of carbon atoms of the adlayer. The present MEIS result indicates that each Si- or C-adlayer making the (3×3) surface reconstruction because the C-Si bilayer is strongly bonded. However, the 1st C layer of the top C-Si bilayer may be distorted to some extent. The probable surface structures are discussed later.

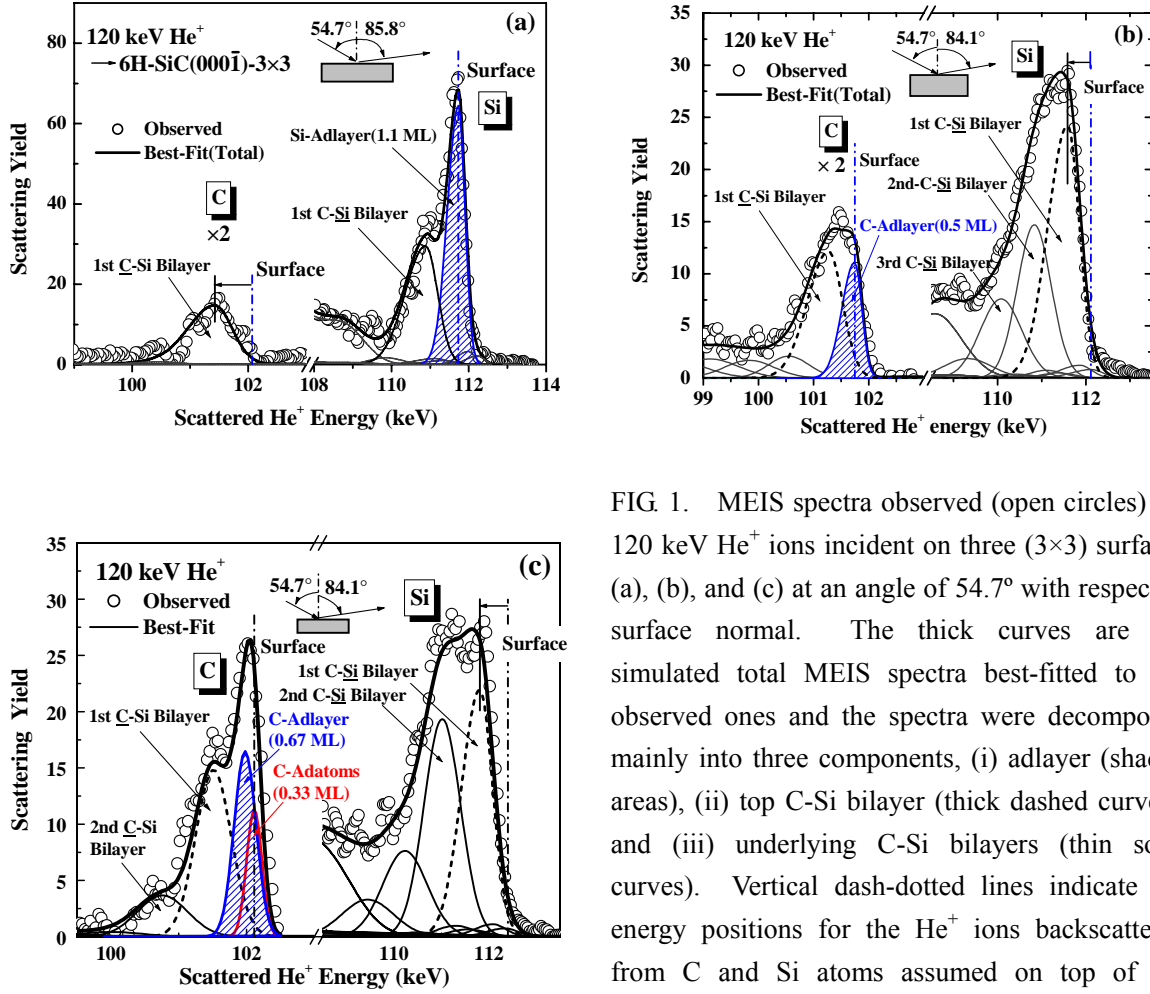


FIG. 1. MEIS spectra observed (open circles) for 120 keV He^+ ions incident on three (3×3) surfaces (a), (b), and (c) at an angle of 54.7° with respect to surface normal. The thick curves are the simulated total MEIS spectra best-fitted to the observed ones and the spectra were decomposed mainly into three components, (i) adlayer (shaded areas), (ii) top C-Si bilayer (thick dashed curves), and (iii) underlying C-Si bilayers (thin solid curves). Vertical dash-dotted lines indicate the energy positions for the He^+ ions backscattered from C and Si atoms assumed on top of the surface.

B. PES Analysis

The chemical bonding states and the electronic nature of the surface are intimately related to the surface structure. So, we measured the C 1s and Si 2p core levels and valence band spectra. Figure 2 shows the Si 2p spectra taken at photon energies of 140 and 280 eV (2nd harmonic). From the top to the bottom, the spectrum becomes more surface sensitive. For the sample (a), three components are seen, bulk and surface-related ones (S1 and S2). The component S1 with a lower binding energy (E_B) relative to the bulk comes from the Si-adlayer, which was confirmed by MEIS. The weak component S2 with a higher E_B value originates from oxidized Si atoms on top (Si-adlayer). This Si-rich surface is active to oxidation reaction. The amount of oxygen was estimated to be about

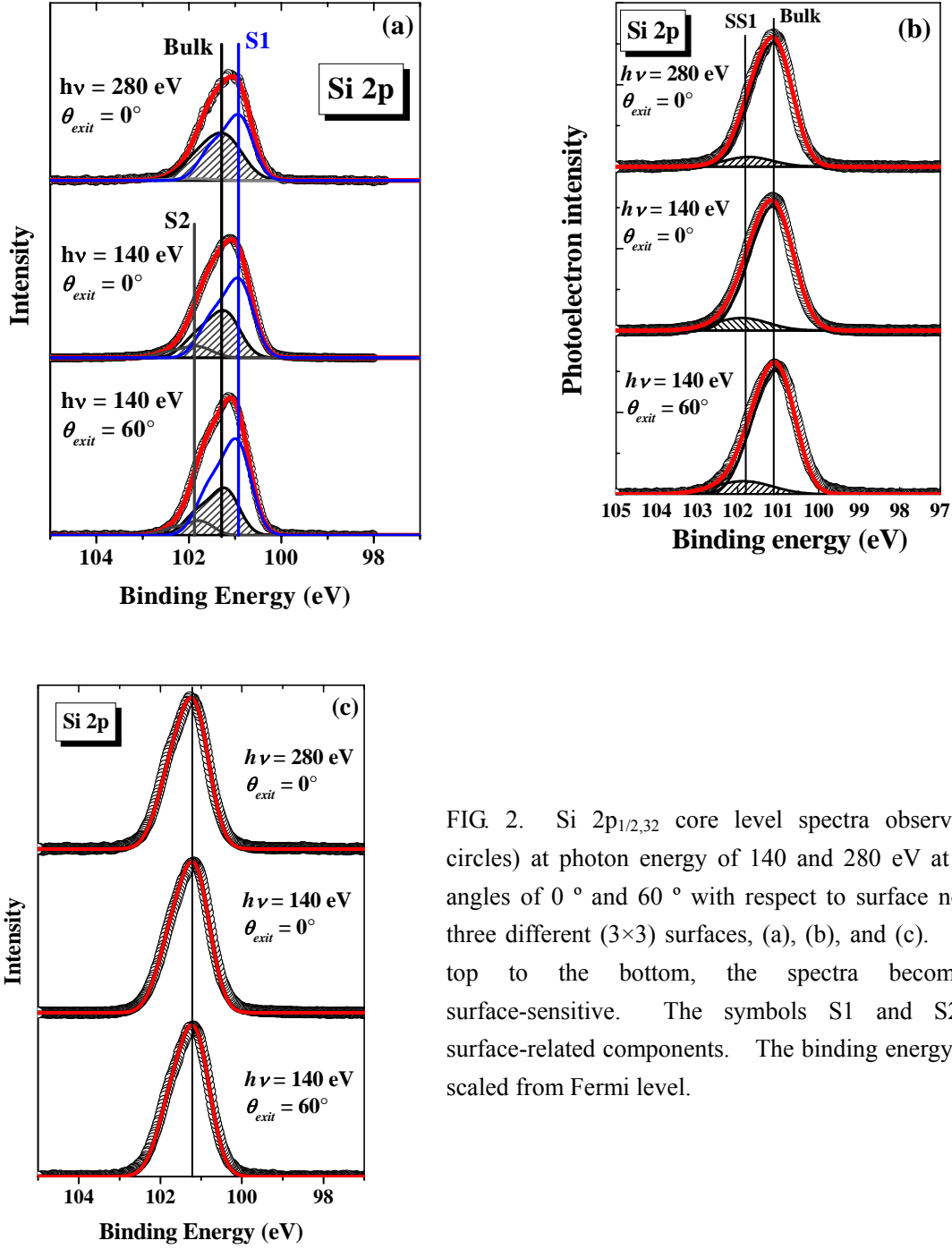


FIG. 2. Si $2p_{1/2,3/2}$ core level spectra observed (open circles) at photon energy of 140 and 280 eV at emission angles of 0° and 60° with respect to surface normal for three different (3×3) surfaces, (a), (b), and (c). From the top to the bottom, the spectra become more surface-sensitive. The symbols S1 and S2 denote surface-related components. The binding energy (E_B) was scaled from Fermi level.

0.1 ML from MEIS analysis. In the cases of the C-rich surfaces ((b) and (c)), we observed only single peak (bulk). This is quite consistent with the MEIS result that the C-adlayer (0.5 ML for (b) and 1.0 ML for (c)) is located on the 1st C-Si bilayer. Each peak position and the width (full width at a half maximum: FWHM) are indicated in Table I. A minor component seen for sample (b) at a higher binding energy comes from a small

Table I. Characteristics of Si $2p_{1/2,3/2}$ and C 1s core levels spectra and valence band measured for three types of SiC(000 $\bar{1}$)- 3×3 surfaces (a), (b), and (c). Absolute amount of each adlayer determined by MEIS is also included.

(i) Sample (a)

Si $2p_{3/2}$ (Peak) (Width: FWHM)	101.20 eV (Bulk) (0.75 eV)	- 0.30 eV (S1) (0.70 eV)	+ 0.60 eV (S2): oxide (0.75 eV)
C 1s (Width: FWHM)	282.9 eV (Bulk) (1.05 eV)		
Valence Band	Semiconductor	Dangling Bond: 1.4 eV	
MEIS	Si-adlayer (1.1 ML)		

(ii) Sample (b)

Si $2p_{3/2}$ (Peak) (Width: FWHM)	101.10 eV (Bulk) (0.75 eV)	+ 0.7 eV (SS1): silicate	
C 1s (Width: FWHM)	283.05 eV (Bulk) (1.0 eV)	+ 1.05 eV (SC1) (1.0 eV)	+ 1.80 eV (SC2) (1.2 eV)
Valence Band	Semiconductor	Broad surface state band	
MEIS	C-adlayer (0.5 ML)		

(iii) Sample (c)

Si $2p_{3/2}$ (Peak) (Width: FWHM)	101.15 eV (Bulk) (0.75 eV)		
C 1s (Width: FWHM)	283.1 eV (Bulk) (1.0 eV)	+ 0.6 eV (SC1') (1.15 eV)	+ 2.25 eV (SC2') (1.25 eV)
Valence Band	Semiconductor	Broad surface state band	
MEIS	C-adatoms(1/3 ML)/C-adlayer(2/3 ML)		

amount of residual silicate domains. Johansson et al.[1] also observed single peak ($E_B = 101.1$ eV) suggesting only one type of Si sites. Their sample prepared is probably similar to our sample (c).

We also observed the C 1s spectra, as shown in Fig. 3. As expected, we observed a single peak for the sample (a), because the 1st C-Si bilayer is covered with a Si-adlayer (1.1 ML). In contrast, there are two surface-related components denoted by (SC1 and SC2) for sample (b) and (SC1' and SC2') for sample (c) other than the bulk component. Note that the bulk-truncated 1st C-Si bilayer is covered by a C-adlayer with thickness of 0.5 and 1.0 ML for the sample (b) and (c), respectively. Emission angle (θ_{exit}) dependence of the

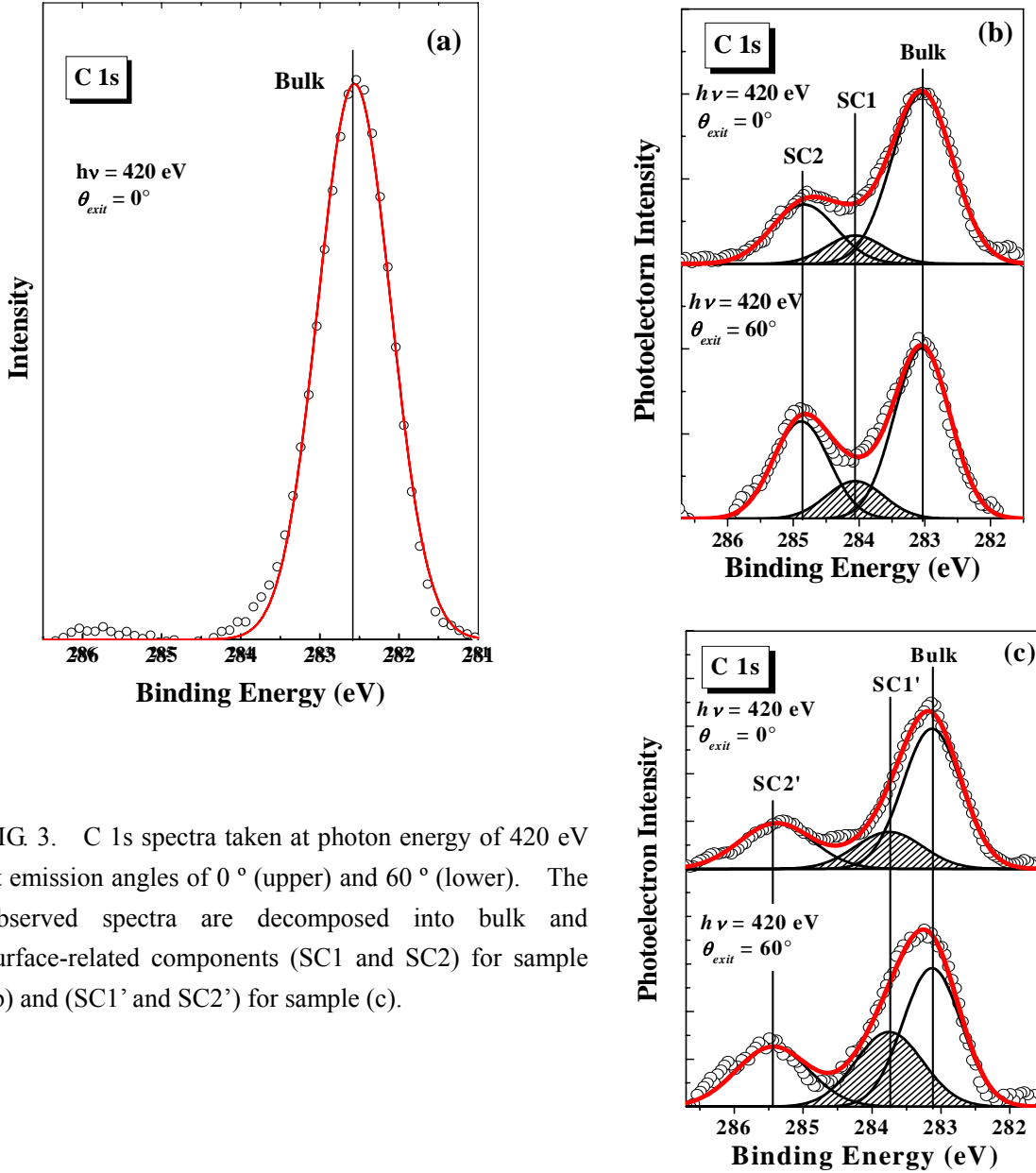


FIG. 3. C 1s spectra taken at photon energy of 420 eV at emission angles of 0° (upper) and 60° (lower). The observed spectra are decomposed into bulk and surface-related components (SC1 and SC2) for sample (b) and (SC1' and SC2') for sample (c).

intensity ratios of SC1(SC1') and SC2(SC2') relative to the bulk gives an evidence that these additional peaks come from surface-related components. In fact, the ratios of SC1(SC1')/bulk and SC2(SC2')/bulk are 14.5(34.8) and 37.9(50.9) % at $\theta_{exit} = 0^\circ$ and 23.4(71.4) and 56.9(76.1) % at $\theta_{exit} = 60^\circ$. The present result that the ratios of SC1(SC2)/bulk are significantly smaller than those of SC1'(SC2')/bulk is due to smaller coverage of C for sample (b) than that for (c). The sample surface (b) is partly covered with the (3×3) domains, because the RHEED spots observed for sample (b) are significantly

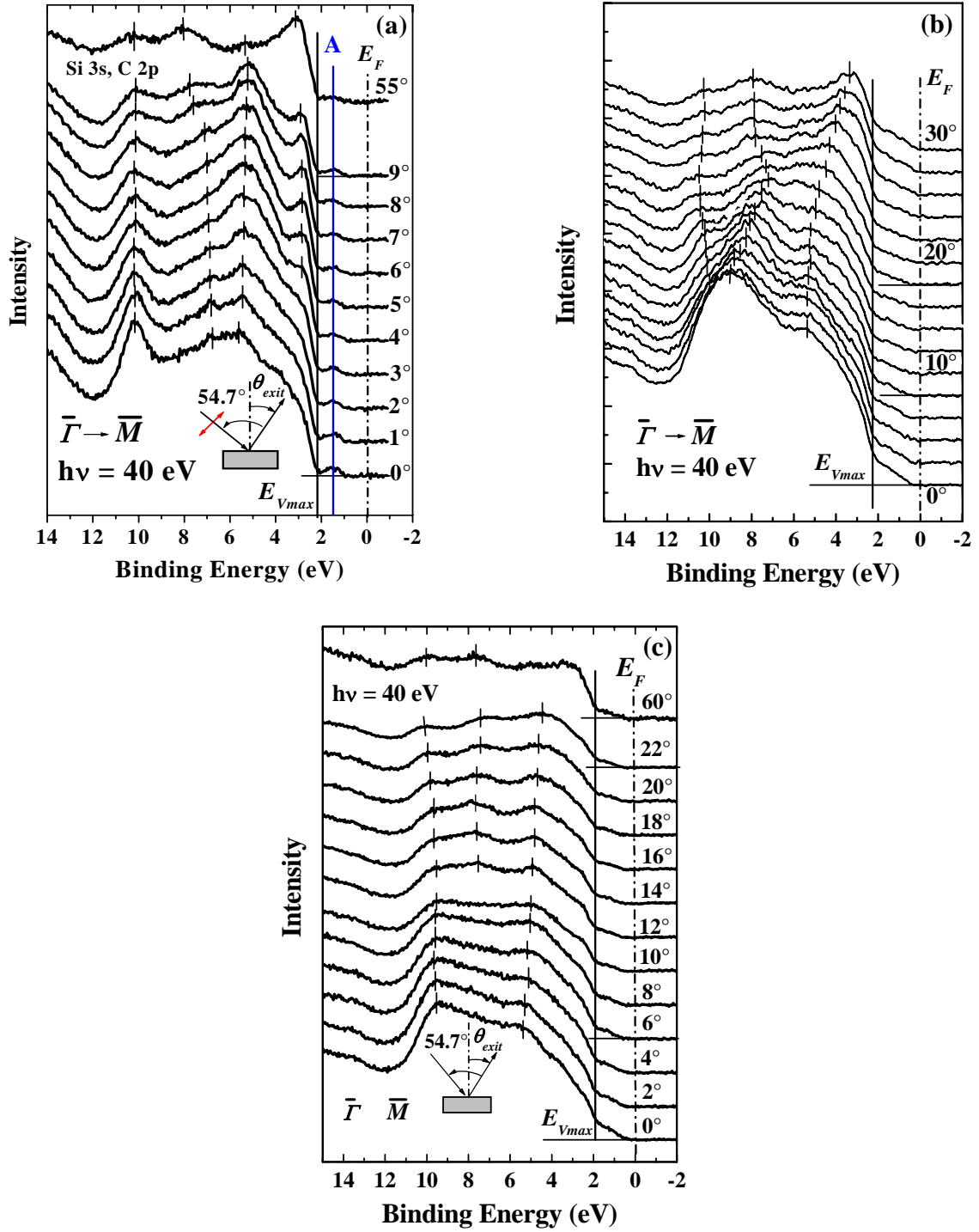


FIG. 4. Valence band spectra observed by varying emission angle for three different (3×3) surfaces, (a), (b), and (c). Incident photon energy and angle between incident beam axis and detection direction was fixed to 40 eV and 54.7° , respectively. The incident photon was p -polarized, as indicated by red arrows. Photons were incident along the $[1\bar{1}00]$ -axis and thus dispersion from $\bar{\Gamma}$ to \bar{M} were obtained.

weak compared with those for samples (a) and (c). It is noteworthy that in the C-Si bonds electrons are transferred from Si to C, because the E_B value of Si 2p for SiC is shifted toward a higher binding energy by 1.2 - 1.5 eV than that for Si[16]. Actually, the C 1s spectrum from HOPG (highly-oriented pyrolytic graphite) graphite (not shown here) has two peaks, primary one (G1) at $E_B = 284.25$ eV(FWHM: 0.8 eV) and additional one (G2) at 284.9 eV(FWHM: 1.65 eV). The E_B values of SC1 and SC2 are close to those of G1 and G2 of graphite. So, the C-adlayer on top of the sample (b) may take a graphite-like structure, while that of the sample (c) is apparently different from graphite. The C atom in the 1st C-Si bilayer is bonded to three Si atoms and one C-atom (the bulk C atom is bonded to four Si atoms). Therefore, the E_B value is expected to be slightly higher than that of the bulk. However, the relatively small core level shift of graphite (1.1 - 1.2 eV) suggests the C 1s peak denoted by 'bulk' containing the component from the 1st C-Si bilayer. Johansson et al.[1,17] observed C 1s spectra which consist of three components, bulk (283.2 eV), two surface-related ones (284.9 and 283.8 eV). They assigned the peak at E_B of 284.9 eV to a carbon sites in a top layer and the broad peak (FWHM: 2.1 eV) at 283.7 eV to an underlying C layer containing inequivalent carbon sites(extrinsic). These E_B values of the surface-related components are significantly different from those observed for the sample (c). The discrepancy probably arises from delicate difference in the sample preparation and annealing process. In fact, this (3×3) pattern sometimes appears not always by annealing at temperatures around 1050 °C for the as-introduced samples without Si deposition. To form this structure, it needs a well-defined and careful annealing procedure. The surface composites grown are dependent also on surface treatment in the air. Sieber et al.[5] observed C 1s spectra for the SiC(000 $\bar{1}$)-3×3 formed by annealing the hydrogen terminated surface at 950°C and found two surface-related components with higher binding energy shifts of 1.05 and 1.81 eV. These values coincide well with those measured for the sample (b).

Finally, we observed the valence band spectra varying emission angle and incident photon energy. Figure 4 shows the valence band spectra at photon energy of 40 eV, as a

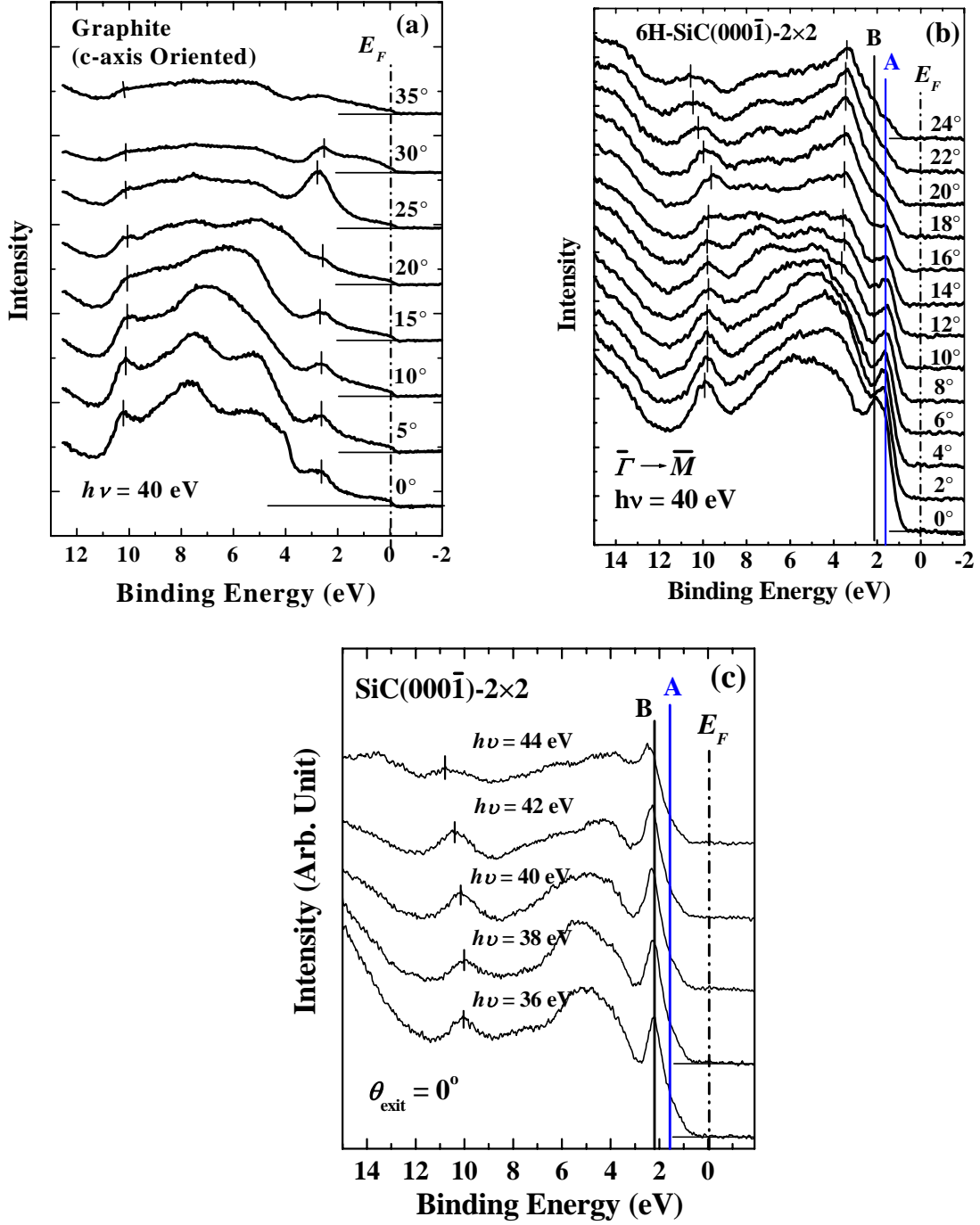


FIG. 5. Valence band spectra observed for c-axis-oriented graphite (a) and Si-rich-SiC(000 $\bar{1}$)-2 \times 2 varying emission angle (b) and varying incident photon energy at normal emission (c). Incident photon energy and angle between incident beam axis and detection direction was fixed to 40 eV and 54.7° , respectively. Incident beam axis, polarization vector (\vec{E}), and detection axis were placed in the horizontal plane (p -polarization).

function of emission angle (θ_{exit}) scaled from surface normal. The incident photon is p -polarized and the angle between the incident beam axis and detection direction was fixed to 54.7° . For the Si-rich surface (a), the band structure corresponds to a semiconductor and a surface state band is clearly seen in the band gap at 1.4 eV below the Fermi level. The peak is non-dispersive and with increasing θ_{exit} the intensity decreases, indicating a p_z character (p_z : an electron orbital (p-state) expanded perpendicularly toward the vacuum, z -axis: surface normal. See Appendix). In addition, exposure to oxygen decreases the peak intensity. Therefore, it is reasonable to regard this surface state band as the dangling bond of the Si-adlayer. The valence band features for the C-rich surfaces ((b) and (c)) also show semiconducting characters. The spectra near the Fermi edges are apparently different from those observed for graphite (see Fig. 5(a)) and double layer of HOPG-like graphite[18] which have a semi-metallic nature. Such difference is due to a single layer of the graphite-like domains and its coverage of a half for the sample (b). The tails toward the Fermi level observed here seem to contain broad surface states bands, which originate from C dangling bonds because of the polarization dependence and no dispersive nature. Of course, the valence band feature of sample (b) is basically different from that of sample (c). For comparison, the valence band spectra observed for the $6H\text{-SiC}(000\bar{1})\text{-}2\times 2$ (Si-rich) surface are shown in Figs. 5(b) and (c). Apparently, the peaks observed in the band gap at 1.6 and 2.1 eV below the Fermi level are non-dispersive and exhibits a p_z character, corresponding to Si- and C-dangling bond states[7]. The Si-rich (2×2) surface has one Si- and one C-dangling bonds in the 2×2 unit cell[7].

C. Probable Surface Structures

Based on the present MEIS and PES results, we discuss probable surface structures for three different types of $\text{SiC}(000\bar{1})\text{-}3\times 3$ reconstructions. An adlayer or adatoms/adlayer taking the (3×3) reconstruction has a C_{3v} symmetry and the absolute amount of the adlayer or adatom/adlayer is estimated to be below 1.2 ML. So, we consider the following atomic configurations (see Figs.6(a)-(d)), as the candidate of the (3×3) reconstructions[19-22].

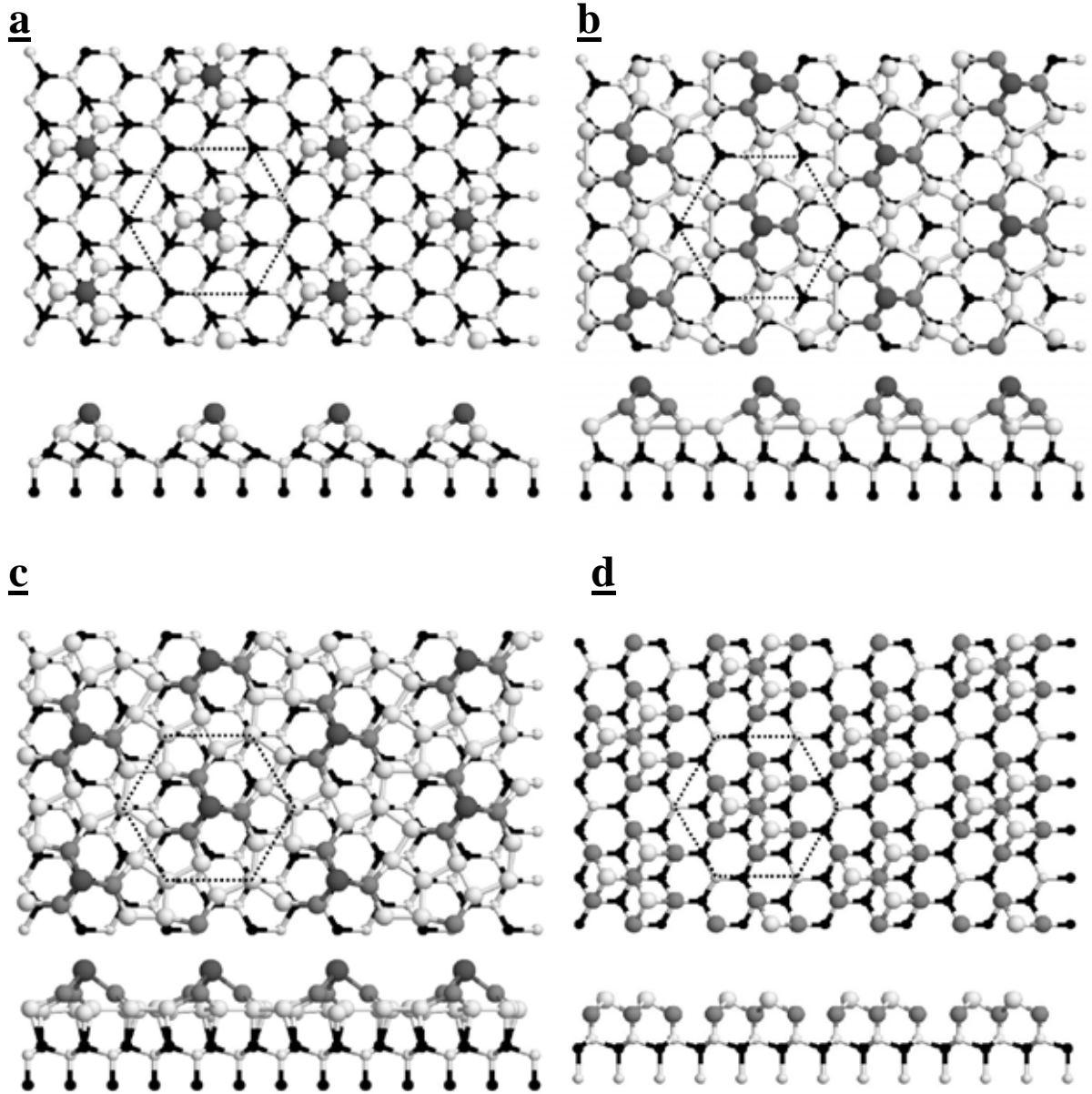


FIG. 6. Top and side views of the models for reconstructed surface structure of $\text{SiC}(000\bar{1})\text{-}3\times 3$. (a) Li-Tsong[20], (b) Klakov[21], (c) Strake[19] and (d) Hoster[6] models. The largest circles denote adatoms and small open-black and full-black circles indicate 1st $\underline{\text{C}}\text{-Si}$ and 1st $\text{C-}\underline{\text{Si}}$ bilayers, respectively. The adtom missing in the Klakov model corresponds to the Hoster model.

Unfortunately, we do not have a probe to observe local structures such as STM and atomic force microscope (AFM) and thus the discussion may be somewhat speculative. The models (a)-(c) were proposed for the $\text{SiC}(0001)\text{-}3\times 3$ surface. Therefore, careful discussions should be done for $\text{SiC}(000\bar{1})\text{-}3\times 3$ considering different bond lengths of

Si-Si(2.35 Å), Si-C(1.88 Å) and C-C(1.54 Å for diamond, 1.43 Å in the layer of graphite). In the Li and Tsong model[20], the surface covered by a trimer of three Si atoms bonded to one Si adatom on top. If this model is applied to the SiC(000 $\bar{1}$)-3×3 surface replacing Si by C atoms, the absolute amount of additional C atoms is 4/9 ML. Of course, the underlying C-layer (1st C-Si bilayer) may be significantly distorted. In the Klakov[21] and Starke[19] models, the bulk-truncated surface is covered with 11/9 and 13/9 ML atoms, respectively. Hoster et al.[6] observed the 6H-SiC(000 $\bar{1}$)-3×3 surface by STM and low energy electron diffraction (LEED) and proposed the structure model that the (3×3) surface takes a hexagonal unit cell consisting of a central trimer bonded to underlying six-atom dimmers rings. Basically, this surface structure corresponds to the Klakov model with missing Si-adatom on top. Their sample was prepared by heating the surface pre-deposited with Si at 1200-1300 °C and corresponds to our sample (a), although the annealing temperature seems too high compared with that in the present experiment (1030 °C) and the report of Bernhardt et al.[2](1000 °C). Such high annealing temperatures that they needed are probably due to excess Si deposition. According to their model, the surface is covered with 1/3 ML of Si-adatoms (trimer) and 7/9 ML of Si-adlayer. They identified the atomic species of adatoms as Si from a relative Auger intensity of about 6 for Si(LVV)/C(KLL). Unfortunately, we could not resolve such a Si-adatoms/Si-adlayer structure, indicating slight difference in heights of the adatoms and adlayer.

Now, we consider the probable surface structures based on the present MEIS and PES results referring to above structure models. In the case of the Si-rich (3×3) surface (a), the bulk truncated surface is covered with 1.1±0.05 ML Si atoms and there are one surface-related component other than the bulk in the Si 2p spectra and one component in the C 1s spectra. So, the Klakov and Hoster models are probable candidates for the Si-rich (3×3) surface (a). Here, we must note that there are three dangling bonds (two in the 1st C-layer and one Si-adatom) in the Klakov model and five dangling bonds (three of an Si trimer and two in the 1st C-layer) in the Hoster model. The surface state band observed at 1.4 eV below Fermi level (see Fig. 4(a)) for the sample (a) probably originates from the

Si-dangling bond, because a similar surface state bands were also observed for the Si-rich SiC(0001)-3×3 (0.9 eV below Fermi level, not shown here) and SiC(000 $\bar{1}$)-2×2 (see Figs. 5(b) and (c)). From the number of the dangling bonds, the Klakov model seems preferable. However, not only dangling bonds but also lattice distortion (bond length) contributes to the total energy of the surface reconstruction. The STM observation by Hoster, Kulakov, and Bullemer[6] showed no Si-adatom on top. In addition, the amount of the adlayer-Si atoms determined by MEIS is 1.1 ± 0.05 ML is close to that of the Hoster model (10/9 ML) and significantly smaller than that of the Klakov mode (11/9 ML). So, the SiC(000 $\bar{1}$)-3×3 surface (a) may take the reconstruction likely the Hoster model, despite many dangling bonds.

It is difficult to identify probable surface structures for the C-rich (3×3) surfaces. From the MEIS result for the sample (b) with C-adatoms of 0.5 ± 0.1 ML (b), the structure of C-trimer bonded to one C-adatom on top (Li-Tsong model) seems to be the most probable candidate. However, due to too short C-C bond length, such a structure cannot give stable atomic configurations. This is confirmed by the first principles calculations[23]. The present PES and RHEED results suggest that the surface of the sample (b) consists partly of graphite-like domains and of a small amount of residual silicate ones. This structure is not very stable, because heating this (3×3) surface at 1100 °C leads to the C-rich (2×2) reconstruction. Here, a question arises how the C-rich (3×3) surface is transformed into the C-rich (2×2) surface consisting of a single Si atom per unit cell in an H₃ site[3], because it is known that annealing at higher temperatures leads to a gradual depletion of Si. Note that annealing at temperatures above 1150 °C graphitizes the surface. Therefore, the present analysis suggests that annealing the sample (a) at 1100 °C breaks the (3×3) domains (a precursor of graphite?) partly covering the surface together with the 1st \bar{C} -Si bilayer to form the C-rich (3×3) surface.

The (3×3) surface of the sample (c) takes C-adatoms(1/3 ML)/C-adlayer(2/3 ML) structure. Unfortunately, however, it is also difficult to determine the surface structure, because of no STM observation for this surface. As mentioned before, the (3×3) pattern

sometimes appears not always by annealing at temperatures around 1050 °C for the as-introduced samples without Si deposition and the C 1s core level spectra observed here are different from those reported by Johansson et al.[1,17]. To form this (3×3) structure it needs a delicate annealing procedure and some surface complex such as disordered carbon clusters may grow by different surface treatments in the air. The absolute amount of the C-adlayer(1 ML) suggests the atomic configuration of the Hoster model replacing the surface Si atoms by C atoms. However, as mentioned before, too short C-C bond length makes such a surface atomic configuration unstable[23]. Finally, it is emphasized that the (3×3) surface of sample (c) is different from that of sample (b), because (i) different atomic configurations (sample (b): Si-adlayer(0.5 ML) and sample (c): C-adatoms(1/3 ML)/C-adlayer(2/3 ML)), (ii) different C 1s and valence band spectra and (iii) different thermal behavior (sample (b): (3×3) → C-rich (2×2) → graphite-(1×1) and (c): (3×3) → graphite-(1×1)).

IV. CONCLUSION

The atomic and electronic structures of 6H-SiC(000 $\bar{1}$)-3×3 surfaces were analyzed by high-resolution MEIS and SR-PES. The (3×3) surfaces were prepared by (a) annealing the Si-rich (2×2) surface at 1030°C, (b) annealing the $\sqrt{3} \times \sqrt{3}$ silicate surface at 1050°C, and (c) annealing the RCA-treated surface at 1050 °C in UHV. The MEIS analysis reveals the fact that the (3×3) surfaces consist of a Si-adlayer(1.1±0.05 ML), C-adlayer(0.5±0.1 ML) and C-adatoms(1/3 ML)/C-adlayer(2/3 ML) on the 1st C-Si bilayer for the samples (a), (b) and (c), respectively. The present analysis shows that the (3×3) reconstructions of the SiC(000 $\bar{1}$) are categorized into the above three types and take different atomic configurations. The surface with the Si-adlayer (a) is semiconducting and has a dangling bond state at 1.4 eV below the Fermi level. The C-rich (3×3) surfaces ((b) and (c)) have a similar electronic structure near the Fermi edges and also show semiconducting characters. Observation of the C 1s and Si 2p core level spectra shows that the Si-rich surface (a) has the bulk and one surface-related component in Si 2p and single bulk component in C 1s.

In contrast, the C-rich surfaces ((b) and (c)) have single bulk component in Si 2p and two surface-related components other than the bulk in C 1s spectra. Based on the above atomic and electronic structures referring to the models proposed so far for the (3×3) reconstructions of SiC(0001) and SiC(000 $\bar{1}$), we consider the probable surface structures. We conclude that the Si-rich surface (a) probably takes the structure proposed by the Hoster et al., in spite of many dangling bonds (five per unit cell). It is difficult to identify the C-rich (3×3) surfaces of sample (b) and (c). It is unlikely for these surfaces to take the structures of the Li-Tsong, Klakov, and Starke models proposed for the SiC(0001)-3×3 surface, because of too short C-C bond length compared with that of C-Si and Si-Si bonds. In fact, the first principles calculations ruled out the Li-Tsong model. In order to identify unambiguously the structure of the SiC(000 $\bar{1}$)-3×3 surfaces, it is essential to predict the most probable atomic configurations by the *ab initio* first principles calculations. This work is now in progress under collaboration with Advanced Industrial Science and Technology (AIST).

Acknowledgments

The authors would like to thank Prof. H. Namba and Dr. K. Ogawa for maintaining the SORIS Beam-Line. Useful discussions with Dr. S. Tanaka and Dr. M. Kohyama are gratefully acknowledged and special thanks are also due to Dr. T. Okazawa and Mr. Y. Matsubara for their help in carrying out the experiments. This work was partly supported by the Fellowship of the Japan Society for the Promotion of Science (JSPS) for Young Scientists.

References

- [1] L.I. Johansson, P.-A. Glans, and N. Hellgren, *Surf. Sci.* **405** (1998) 288.
- [2] J. Bernhardt, M. Nerding, U. Starke, and K. Heinz, *Materials Sci. Eng.* **B 61-62** (1999) 207.

- [3] A. Seubert, J. Bernhardt, M. Nerding, U. Starke, and K. Heinz, *Surf. Sci.* **454-456**, (2000) 45.
- [4] I. Forbeaux, J.-M. Themlin, and J.-M. Debever, *Surf. Sci.* **442** (1999) 9.
- [5] N. Sieber, Th. Seyler, and L. Ley, *Phys. Rev.* **B 67**, (2003) 205304.
- [6] H.E. Hoster, M.A. Kulakov, and B. Bullemer, *Surf. Sci.* **382** (1997) L658.
- [7] Y. Hoshino, R. Fukuyama, Y. Matsubara, T. Nishimura, S. Tanaka, M. Kohyama, and Y. Kido, *Phys. Rev.* **B 71** (2005) 195331.
- [8] W. Kern and D.A. Poutinen, *RCA Rev.* **31** (1970) 187.
- [9] Y. Hoshino, R. Fukuyama, and Y. Kido, *Phys. Rev.* **B 70** (2004) 165303.
- [10] Y. Kido, H. Namba, T. Nishimura, A. Ikeda, Y. Yan, and A. Yagishita, *Nucl. Instrum. Methods* **B 136-138** (1998) 798.
- [11] J. Lindhard and M. Scharff, *K. Dan Vedensk. Selsk. Mat. Fys. Medd.* **27** (1953) No. 15.
- [12] Y. Hoshino, S. Semba, T. Okazawa, and Y. Kido, *Surf. Sci.* **515** (2002) 305.
- [13] P.L. Grande, A. Hentz, G. Schiwietz, W.H. Schulte, B.W. Busch, D. Starodub, and T. Gustafsson, *Phys. Rev.* **B 69** (2004) 104112.
- [14] Y. Kido, S. Semba, and Y. Hoshino, *Nucl. Instrum. Methods* **B 219-220** (2004) 599.
- [15] J.F. Ziegler, J.P. Biersack, and W. Littmark, *The Stopping and Range of Ions in Matter* (Pergamon, New York, 1985).
- [16] M. Hollering, F. Maier, N. Sieber, M. Stammeler, J. Ristein, L. Ley, A.P.J. Stampfl, J.D. Riley, R.C.G. Leckey, F.P. Leisenberger, and F.P. Netzer, *Surf. Sci.* **442** (1999) 531.
- [17] Y. Hoshino, S. Matsumoto, T. Nakada, and Y. Kido, *Surf. Sci.* **556** (2004) 78.
- [18] C. Virojanadara and L.I. Johansson, *Surf. Sci.* **505** (2002) 358.
- [19] U. Starke, J. Schardt, J. Bernhardt, M. Franke, K. Reuter, H. Wedler, K. Heinz, J. Furthmüller, P. Köckel, F. Bechstedt, *Phys. Rev. Lett.* **80** (1998) 758.
- [20] L. Li and I.S.T. Tsong, *Surf. Sci.* **351** (1996) 141.
- [21] M.A. Klakov, G. Henn, and B. Bullemer, *Surf. Sci.* **346** (1996) 49.
- [22] T. Aoyama, K. Akimoto, A. Ichimiya, Y. Hisada, S. Mukainakano, T. Emoto, H. Tajiri, T. Takahashi, H. Sugiyama, X. Zhang, H. Kawata, *Appl. Surf. Sci.* **216** (2003) 356.
- [23] S. Tanaka and M. Kohyama, private communication.

Appendix

Photoemission intensity P is calculated using the dipole approximation valid for $h\nu \leq 500$ eV. The dipole approximation leads to the expression,

$$P \propto \left| \langle i | \vec{A} \cdot \nabla | f_k \rangle \right|^2 = \left| \vec{A} \cdot \vec{k} \right|^2 \left| \langle i | f_k \rangle \right|^2, \quad (\text{A-1})$$

where \vec{A} and \vec{k} are the vector potential (polarization) of light and the wave vector of emitted electrons, respectively and $|f_k\rangle$ is a final state taking a form $\exp(i k z')$. Here, photoelectrons are emitted along z' -direction (θ_{exit} : emission angle scaled from surface normal (z -axis)) and the angle between \vec{k} and incident photon axis is α , which was fixed to 54.7° in the present experiment. If the electrons of p_z -state are concerned,

$$\langle i | = \psi_{p_z} = R(r) \sqrt{\frac{3}{4\pi}} \cos \theta = R(r) \sqrt{\frac{3}{4\pi}} \{ \cos \theta_{\text{exit}} \cos \theta' + \sin \theta_{\text{exit}} \sin \theta' \}, \quad (\text{A-2})$$

where $R(r)$ is a radial function. The final state is expressed by

$$|f_k\rangle = \exp(i k z') = \sum_l \sqrt{\frac{4\pi}{2l+1}} (2l+1) i^l j_l(kr) Y_{l0}(\theta', \varphi'), \quad (\text{A-3})$$

where $j_l(kr)$ and $Y_{l0}(\theta', \varphi')$ are the Bessel function and spherical harmonics, respectively. Using the orthogonal relation for $Y_{l0}(\theta', \varphi')$, one obtains

$$P \propto \left| \vec{A} \cdot \vec{k} \right|^2 \cos^2 \theta_{\text{exit}}. \quad (\text{A-4})$$

